Biochemical Characterization of Dithiol Glutaredoxin 8 from *Saccharomyces cerevisiae*: The Catalytic Redox Mechanism Redux[†]

Elisabeth Eckers,[‡] Melanie Bien,[§] Vincent Stroobant,[||] Johannes M. Herrmann,[§] and Marcel Deponte*[,‡]

Butenandt Institute for Physiological Chemistry, Ludwig-Maximilians University, D-81377 Munich, Germany, Cell Biology, University of Kaiserslautern, D-67663 Kaiserslautern, Germany, and Ludwig Institute for Cancer Research and Cellular Genetics Unit, Université Catholique de Louvain, B-1200 Brussels, Belgium

Received October 1, 2008; Revised Manuscript Received November 19, 2008

ABSTRACT: Two dithiol glutaredoxins (Grxs), Grx1 and Grx2, from yeast have been characterized to date. A third putative dithiol glutaredoxin-encoding gene (*GRX8*) has been identified *in silico*. Here we show that deletion of *GRX8* does not result in a reduced growth rate under oxidative stress conditions, nor does it enhance the defects of Δ*grx1* and Δ*grx2* single or double mutants. We furthermore compare the enzymatic properties of recombinant *Sc*Grx8 with the monothiol glutaredoxin *Sc*Grx7. Molecular models of *Sc*Grx8 suggest that the protein has a canonical Grx fold, a significantly altered substrate binding site, and a Trp14-type cysteine motif at the catalytic center. *Sc*Grx8 did not bind heavy metal ions and was exclusively monomeric. Apparent k_{cat} values for *Sc*Grx8 in the standard enzymatic assay were about 3 orders of magnitude less than for *Sc*Grx7, whereas apparent K_m values were comparable. Mass spectrometric analyses support a ping-pong mechanism for *Sc*Grx7 and *Sc*Grx8 with a glutathionylated protein as an intermediate. Reduction kinetics of *Sc*Grx8 disulfide, glutathionylated *Sc*Grx8^{C28S}, and glutathionylated *Sc*Grx7 revealed significant differences between the proteins. Surprisingly, mutation of the more C-terminal cysteine residue in the CPDC motif of *Sc*Grx8 also abolished the slight enzymatic activity, and thus the standard catalytic mechanism for glutathionylated substrates does not apply to the enzyme. In summary, *Sc*Grx8 has several novel structural and mechanistic features expanding the subclasses of glutaredoxins. A refined catalytic model for monothiol and dithiol glutaredoxins is presented explaining the diversity of enzymatic activities *in vitro* and pointing to different functions *in vivo*.

Structurally, all Grxs[1] are members of the thioredoxin superfamily because of their "thioredoxin fold". This fold is highly conserved throughout evolution and is comprised of four or five central β-strands surrounded by α-helices (*1*). Grxs are ubiquitous proteins that recognize glutathionylated compounds (e.g., glyceraldehyde-3-phosphate dehydrogenase) and utilize one or two molecules of reduced glutathione (GSH) for reduction of inter- or intramolecular disulfide bonds (Figure 1). The specificity for glutathione distinguishes Grxs from thioredoxins (Trxs). Accordingly, Grxs possess moderately conserved, positively charged amino acids at the active site that interact with the carboxylate group(s) of glutathione. The functionally and mechanistically heterogeneous class of Grxs can be subdivided into mono- and dithiol Grxs depending on the number of cysteine residues at the CxxC/S active site. Further categorization of Grxs is based on different (putative) physiological functions (i), subcellular localizations (ii), and biochemical properties such as the abilities to form noncovalent dimers (iii), to bind iron−sulfur clusters (iv), to form alternative cysteine disulfide bonds (v), or to catalyze reduction of model substrates (vi) (for recent reviews on Grxs see refs *2*−*5*).

Baker's yeast *Saccharomyces cerevisiae* contains two dithiol and five monothiol Grxs that have been studied previously (*2*, *6*−*14*). The monothiol glutaredoxins *Sc*Grx6 and *Sc*Grx7 are unusual because they are membrane-anchored via their N-termini and are found in the secretory pathway, in particular in the *cis* Golgi. Both proteins have enzymatic activity *in vitro* and *in vivo* and could be important to counteract oxidation or glutathionylation of protein thiol groups in the secretory organelles (*12*−*14*). Uncharacterized glutaredoxin-like *Sc*Grx8 has been identified as a putative third yeast dithiol Grx *in silico* (*13*, *15*). The encoding gene is not essential, and *Sc*Grx8 is of low abundance (about 600 molecules per cell) (*16*). A GFP-fusion construct was shown to localize to the cytoplasm (*17*).

Many Grxs are able to catalyze the GSH-dependent reduction of bis(2-hydroxyethyl) disulfide (HEDS) to 2-mercaptoethanol (2-ME) in a coupled enzymatic assay. A

[†] This work was supported by grants from the Deutsche Forschungsgemeinschaft (DFG), De1431/1-1 (to M.D.) and He2803/4-1 (to J.M.H.).

* To whom correspondence should be addressed. Tel: 49-89-2180-77122. Fax: 49-89-2180-77093. E-mail: marcel.deponte@gmx.de.

[‡] Ludwig-Maximilians University.

[§] University of Kaiserslautern.

[||] Université Catholique de Louvain.

[1] Abbreviations: diamide, diazenedicarboxylic acid bis(*N*,*N*-dimethylamide); DTT, dithiothreitol; Grx(s), glutaredoxin(s); *Sc*Grx/*Ec*Grx, glutaredoxin from *Saccharomyces cerevisiae* or *Escherichia coli*; Grx(S_2), glutaredoxin disulfide; Grx-SSG, glutathionylated Grx; GR, glutathione reductase; GSH, reduced glutathione; GSSG, glutathione disulfide; HEDS, bis(2-hydroxyethyl) disulfide; IAc, iodoacetamide; 2-ME, 2-mercaptoethanol; GSSEtOH, mixed disulfide between GSH and 2-ME; GSSCys, L-cysteine−glutathione disulfide; Ni-NTA, nickel−nitrilotriacetic acid agarose; Trx(s), thioredoxin(s); TrxR, thioredoxin reductase.

10.1021/bi801859b CCC: $40.75
Published on Web 01/23/2009

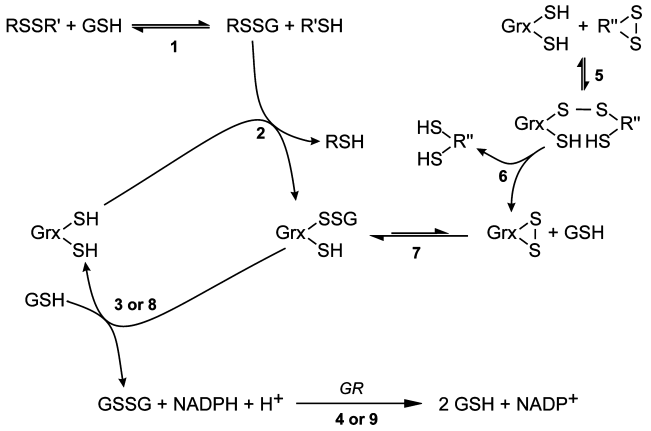

FIGURE 1: Model of the catalytic mechanism of dithiol Grxs. Substrates for Grxs either contain a glutathionylated thiol group that can be formed nonenzymatically (step 1) or a (intramolecular) disulfide bond that is specifically recognized. Reduction of glutathionylated substrates occurs via a ping-pong mechanism comprising a single oxidative half-reaction (step 2) and a GSH-dependent reductive half-reaction (step 3) with respect to Grx. The latter leads to formation of GSSG which is reduced by NADPH with the help of glutathione reductase (GR) (step 4). Specific reduction of protein disulfide substrates occurs via a disulfide exchange mechanism yielding reduced substrate and Grx disulfide during the oxidative half-reaction (steps 5 and 6). The reductive half-reaction comprises glutathionylation of the more N-terminal cysteine residue of the CxxC motif (step 7) and subsequent GSSG formation (step 8) which is finally followed by NADPH consumption (step 9).

significant activity in the HEDS assay was detected for the dithiol Grxs from different organisms such as *Escherichia coli* (*18*−*21*), mammals (*19*, *21*−*27*), *Oryza sativa* (*28*), *Saccharomyces cerevisiae* (*6*), *Plasmodium falciparum* (*29*), *Populus trichocarpa* (*30*), and *Chlamydomonas reinhardtii* (*31*). With the exception of *Sc*Grx6 and *Sc*Grx7 (*12*−*14*), monothiol Grxs were found to be inactive in this assay (*10*, *31*−*34*).

The widely accepted catalytic mechanism for dithiol Grxs during reduction of glutathionylated substrates starts with the nucleophilic attack of the thiolate group of the more N-terminal cysteine residue in the CxxC motif (Figure 1). As a result, deglutathionylated product is released, and a mixed disulfide between glutathione and the active site cysteine residue of Grx is formed (Grx-SSG). During the reductive part of the ping-pong reaction, free GSH regenerates reduced glutaredoxin ($Grx(SH)_2$), yielding oxidized glutathione (GSSG) as the second product. Please note that the more C-terminal cysteine residue at the active site is not required in this mechanistic model for glutathionylated substrates. NADPH-dependent reduction of GSSG is finally catalyzed by the flavoprotein glutathione reductase (GR) (*27*, *35*−*38*). We recently performed kinetic studies on the natural monothiol glutaredoxin *Sc*Grx7 using GSH and L-cysteine−glutathione disulfide (GSSCys) as substrates. Kinetic patterns with GSSCys supported a ping-pong mechanism, and therefore the occurrence of a *Sc*Grx7-SSG intermediate during catalysis was postulated (*12*). Here we provide experimental evidence for this reaction intermediate. Furthermore, we describe the novel monomeric dithiol glutaredoxin *Sc*Grx8 from yeast and compare enzymatic properties with *Sc*Grx7. Surprisingly, *Sc*Grx8 has very low activity in the HEDS assay and requires both active site cysteine residues for catalysis. Our results point to conformational changes in *Sc*Grx7 and *Sc*Grx8 and lead to the formulation of a more detailed catalytic mechanism that is in accordance with previous observations on mono- and dithiol Grxs.

MATERIALS AND METHODS

All chemicals used were of the highest purity available. Glutathione reductase from yeast, GSH, GSSG, dithiothreitol (DTT), and NADPH were obtained from Sigma, HEDS was from Alfa Aesar, recombinant human insulin was from Roche, and *E. coli* Trx (*Ec*Trx) and yeast thioredoxin reductase (TrxR) were from Merck. PCR primers were obtained from Metabion, and Ni-NTA agarose resin was purchased from Qiagen. Recombinant *Sc*Grx7 was purified as described previously (*12*).

Cloning and Site-Directed Mutagenesis. Using the *Saccharomyces* genome database (http://www.yeastgenome.org/) an open reading frame encoding an uncharacterized nonessential dithiol glutaredoxin on chromosome XII was previously identified *in silico* (*13*) (SGD annotation YLR364W). A full-length construct of *SCGRX8* was PCR-amplified from genomic DNA and cloned into pQE30 (Qiagen) using the primers 5′-GACTGGATCCGCCTTTGTTACTAAAGCTGAAGAG-3′ (ScGrx8/*Bam*HI/s) and 5′-GACTAAGCTTTCAAGGCAGAAGCCCGATTTTAGTC-3′ (ScGrx8/*Hin*dIII/as). Active site mutations of $SCGRX8^{C25S}$ and $SCGRX8^{C28S}$ were introduced by PCR using mutated primers (ScGrx8/C25S/s 5′-GTTATCCGCCAGCTGGAGCCCCGACTGCGTCTATG-3′, ScGrx8/C25S/as 5′-CATAGACGCAGTCGGGGCTCCAGCTGGCGGATAAC-3′, ScGrx8/C28S/s 5′-CAGCTGGTGCCCCGACAGCGTCTATGCTAATTCC-3′, and ScGrx8/C28S/as 5′-GGAATTAGCATAGACGCTGTCGGGGCACCAGCTG-3′). Methylated nonmutated template plasmids were digested with *Dpn*I (Promega), and competent *E. coli* XL1-Blue cells were subsequently transformed. All PCR reactions were performed with *Pfu* polymerase (Promega), and correct insertions and sequences of wild type and mutant constructs were confirmed by sequencing both strands.

Yeast Strains and Growth Media. All strains used in this study were isogenic to the wild-type strain YPH499 (Mat a *ura3 lys2 ade2 trp1 his3 leu2*) (*39*). For generation of deletion mutants of *GRX1*, *GRX2*, *GRX8*, or combinations of those, the entire coding regions of the genes were replaced by *URA3*, kanamycin resistance, and *HIS3* cassettes, respectively. Yeast cultures were grown at 30 °C in YP (1% yeast extract, 2% peptone) medium supplemented with 2% glucose (YPD) or in minimal medium supplemented with 20 μg/mL adenine, uracil, histidine, and tryptophan and 30 μg/mL leucine and lysine (*40*).

Heterologous Expression, Protein Purification, and Detection. N-Terminally $MRGS(H)_6G$-tagged proteins were expressed in *E. coli* strain XL1-Blue. Competent cells were transformed prior to each experiment, and suspension cultures were grown at 37 °C to an optical density at 600 nm of 0.5 in Luria−Bertani (LB) medium containing 100 μg/mL ampicillin. Expression was subsequently induced for 4 h by adding 0.5 mM isopropyl β-D-1-thiogalactopyranoside. Cells from 1 L of culture were harvested by centrifugation at 4 °C (15 min, 4000*g*), washed, and resuspended in 10 mL of buffer containing 50 mM sodium phosphate, 300 mM NaCl,

and 10 mM imidazole, pH 8.0. Cell walls were digested with lysozyme followed by sonication on ice. The suspension was centrifuged at 4 °C (60 min, 30500*g*) and loaded on a column containing nickel−nitrilotriacetic acid agarose (Ni-NTA). Recombinant *Sc*Grx8 was eluted with the same buffer containing 125 mM imidazole. Protein concentrations of the eluates were determined using the Bradford assay with bovine serum albumin as a standard (*41*). Samples were analyzed by gel filtration chromatography (see below) and by reducing and nonreducing SDS−PAGE (*42*).

Metal Content Analyses. The metal content of *Sc*Grx8 freshly purified from *E. coli* was analyzed in a central facility of the Ludwig-Maximilians University by inductively coupled plasma atomic emission spectroscopy (ICP-AES) using a Varian Vista RL CCD simultaneous ICP-AES spectrometer and the software ICP expert.

HPLC and Mass Spectrometry. For the mass spectrometry (MS) analysis, proteins or enzymatically digested peptides were injected on a reverse-phase chromatography PepMap C18 0.3/15 column (LC Packings, Sunnyvale, CA) and eluted with a 35 min linear gradient of acetonitrile in water (5−50%) containing 0.05% TFA with a flow rate of 4 μL/min. The MS analysis was performed on line with a LCQ Deca XP ion-trap spectrometer equipped with an electrospray ionization source (ThermoFinnigan, San Jose, CA). The LCQ was operated in positive mode under manual control in the Tune Plus view with default parameters and active automatic gain control.

Gel Filtration Chromatography. Oligomerization of *Sc*Grx8 was studied by gel filtration chromatography on a HiLoad 16/60 Superdex 200 prep grade column, which was connected to an ÄKTA-FPLC system (GE Healthcare). The column was calibrated with a gel filtration standard (GE Healthcare) and equilibrated with buffer containing 50 mM sodium phosphate and 300 mM NaCl, pH 7.4, with or without 2 mM GSH. FPLC fractions were detected photometrically, and peak areas and k_{AV} values were evaluated using the software UNICORN 3.21 (GE Healthcare). Protein-containing FPLC fractions were analyzed by reducing and nonreducing SDS−PAGE.

Reduction and Oxidation Studies. For several experiments *Sc*Grx8 was reduced in the absence of additional thiol-containing agents by adding $NaBH_4$ at a ∼50-fold molar excess. $NaBH_4$ was dissolved in a NaOH solution, pH 10, prior to each experiment. Salt concentrations and pH of the protein sample did not change significantly after addition of the $NaBH_4$-containing solution. After 1.5−3 h incubation at room temperature excess $NaBH_4$ was degraded (*43*) as confirmed by DTNB assays (see below). In order to generate *Sc*Grx8 disulfide (*Sc*Grx8(S_2)), 0.5 mM freshly purified protein was incubated with 10 equiv of diazenedicarboxylic acid bis(*N*,*N*-dimethylamide) (diamide) (*44*) for 2 h at room temperature. Alternatively glutathionylated *Sc*Grx8^{C28S} and glutathionylated homogeneous S*c*Grx7 (*Sc*Grx7-SSG) were obtained after incubation of freshly purified protein with a 100-fold molar excess of GSSG overnight at 4 °C. Precipitated protein was removed by centrifugation, and oxidized *Sc*Grx8(S_2) or glutathionylated protein was subsequently repurified by Ni-NTA chromatography and concentrated in a Centriprep YM-10 (Millipore).

DTNB Assays. Unmodified thiol groups of 20 μM untreated, reduced, oxidized, and aged *Sc*Grx8 were quantified with 5,5′-dithiobis(2-nitrobenzoic acid) (DTNB) (*45*). In parallel, 2-mercaptoethanol (0−80 μM) was used for calibration curves. All assays were performed in elution buffer containing 0.6 mM DTNB, with or without 5% SDS, and 2 mM EDTA. Samples were incubated for 10 min at room temperature before the liberation of 5-thio-2-nitrobenzoate was detected at 412 nm.

Glutathione:HEDS and Glutathione:GSSCys Thioltransferase Assays. Steady-state kinetics of *Sc*Grx8 and *Sc*Grx7 were monitored spectrophotometrically at 25 °C with a thermostated Jasco V-550 UV/vis double beam spectrophotometer. Stock solutions of 4 mM NADPH, 40−80 mM GSH, 40 units/mL GR, and 29.4 mM HEDS or 10 mM L-cysteine−glutathione disulfide (GSSCys) were freshly prepared in assay buffer (0.1 M Tris-HCl, 1 mM EDTA, pH 8.0) before each experiment. Unless otherwise described, measurements were performed as follows (see also ref *12*): HEDS, GSH, and 0.1 mM NADPH were preincubated in assay buffer for 2 min before 1.0 unit/mL GR was added, and a baseline was recorded for 30 s. The assay was started by the addition of 25 μM *Sc*Grx8. Either the initial concentration of GSH (between 0.1 and 4 mM) was varied at a fixed initial concentration of HEDS (0.74 mM) or the initial concentration of HEDS (between 0.1 and 1.0 mM) was varied at a fixed initial concentration of GSH (2.0 mM). The consumption of NADPH ($\epsilon_{340nm} = 6.22\ mM^{-1}\ cm^{-1}$) was monitored at 340 nm. Measured activities in all assays were corrected (i) by subtracting the absorbance of a reference cuvette containing all components excluding Grx and (ii) by subtracting the slope (ΔAbs/min) of the baseline. Reaction velocities were plotted according to Michaelis−Menten and Hanes and fitted using the program SigmaPlot 10.0 (Systat Software, Inc.). The apparent kinetic parameters K_m^{app} and k_{cat}^{app} were determined by nonlinear regression of Michaelis−Menten plots and by linear regression of Hanes plots. Values for K_m^{app} and k_{cat}^{app} calculated from the different plots of a single experiment usually varied by less than 10%.

ScGrx8 Disulfide, ScGrx8^{C28S}-SSG, and ScGrx7-SSG Reduction Assays. Yeast GR/GSH and yeast TrxR were tested as electron donor systems for oxidized Grx. Assays containing GR/GSH were essentially performed as described above; however, no HEDS was added, and reduced protein was replaced with 0−25 μM *Sc*Grx8 disulfide, *Sc*Grx8^{C28S}-SSG, or *Sc*Grx7-SSG as final electron acceptor. Assays with TrxR were performed without a reference cuvette at 25 °C in buffer containing 100 mM $K_xH_yPO_4$, 1 mM EDTA, pH 7.0, 0.2−0.6 μM TrxR, and 100 μM NADPH. A baseline was recorded for 30 s before the addition of 30 μM *Sc*Grx8 disulfide or 30 μM *Sc*Grx7-SSG. Measured activities were corrected by subtracting the slope of the baseline. Activity of TrxR was confirmed with NADPH and DTNB as substrates.

Turbidimetric Insulin Disulfide Reduction Assay. Reduction of 0.17 mM insulin by 1 mM DTT was analyzed at 25 °C in the absence and presence of *Sc*Grx8 in assay buffer containing 50 mM Tris-HCl and 2 mM EDTA, pH 7.4. Assays with *Ec*Trx (1 or 10 μM) served as positive controls. Samples contained 25 μM or 0.1 mM *Sc*Grx8. The same volume of imidazole-containing elution buffer was added to negative controls. All reactions were started by the addition of DTT, and turbidity was monitored for 80 min at 600 nm (*29*).

Sequence Alignment and Molecular Modeling. The Protein Data Bank was searched for protein structures containing a thioredoxin fold. Sequences of potential templates were aligned with *Sc*Grx8 using the program ClustalW (*46*). A model of *Sc*Grx8 was generated based on the crystal structure of monomeric human Grx2. The protein was selected because of the comparable size, the high sequence similarity, and the bound glutathione molecule (*47*) (Protein Data Bank accession number 2FLS). Alignments between the template and *Sc*Grx8 were optimized manually in the Swiss-PDB Viewer (spdbv). Computations of the models were carried out at the Swiss-Model server using the "optimize (project)" mode (*48*, *49*). The force field energy of the models was calculated with the GROMOS96 implementation of spdbv.

RESULTS

ScGrx8 Does Not Contribute to General Resistance against Oxidative Stress. Glutaredoxins play a pivotal role in maintaining proteins in a reduced, functional state, in particular in the presence of oxidants (*3*−*5*). To assess the relevance of *Sc*Grx8 *in vivo*, we constructed yeast mutants in which the *GRX8* gene was replaced by a *HIS3* cassette. Moreover, we generated combination mutants in which, in addition to the *GRX8* deletion, the reading frames of the genes of the other two dithiol glutaredoxins, *GRX1* and *GRX2*, were replaced by *URA3* or a kanamycin resistance gene (Figure 2A). Neither single nor combination mutants showed reduced growth rates under nonstress conditions (Figure 2B). In contrast, in the presence of hydrogen peroxide, paraquat, or iron chloride, growth defects were observed for strains lacking *GRX1* and *GRX2*. These defects were not further increased by loss of *GRX8*. Furthermore, Δ*grx1* and Δ*grx2* mutants showed a resistance to diamide (*6*) which might be due to the glutaredoxin-dependent formation of a toxic byproduct. The additional deletion of the *GRX8* gene did not further improve this diamide tolerance. Immunoblots of cell extracts of the mutants did not indicate alterations in the levels of the cytosolic thioredoxins Trx1 and Trx2 (data not shown). Thus, the absence of a detectable defect in Δ*grx8* cells was probably not masked by a compensatory upregulation of Trxs. In summary, we conclude that *Sc*Grx8 does not play a significant role in the general oxidative stress defense. The protein might rather be involved in a more specialized function which is not detectable by the conditions used for the growth assays.

Sequence Alignments and Molecular Models Point to a Significantly Altered Active Site of ScGrx8. Using the sequence of *Sc*Grx8 for a BLAST search, highest overall similarities were obtained for dithiol Grxs. *Sc*Grx8 does not have large N- or C-terminal extensions in contrast to many other members of the thioredoxin-fold family. Accordingly, an energetically stable model of the compact full-length protein could be generated (Figure 3A) based on the structure of human Grx2 in complex with glutathione (Figure 3B). Residues Lys^{34} and Gln^{69} of human Grx2 (binding the glycine carboxylate group of glutathione (*47*)) and several residues in α-helix 3 (being probably involved in substrate recognition) are not well conserved in *Sc*Grx8 and putative homologous proteins from other *Saccharomycetes* (Figure 3A,B,D). However, residue Arg^{71} before β-strand 3 of *Sc*Grx8 is conserved (or replaced by a lysine residue) in these

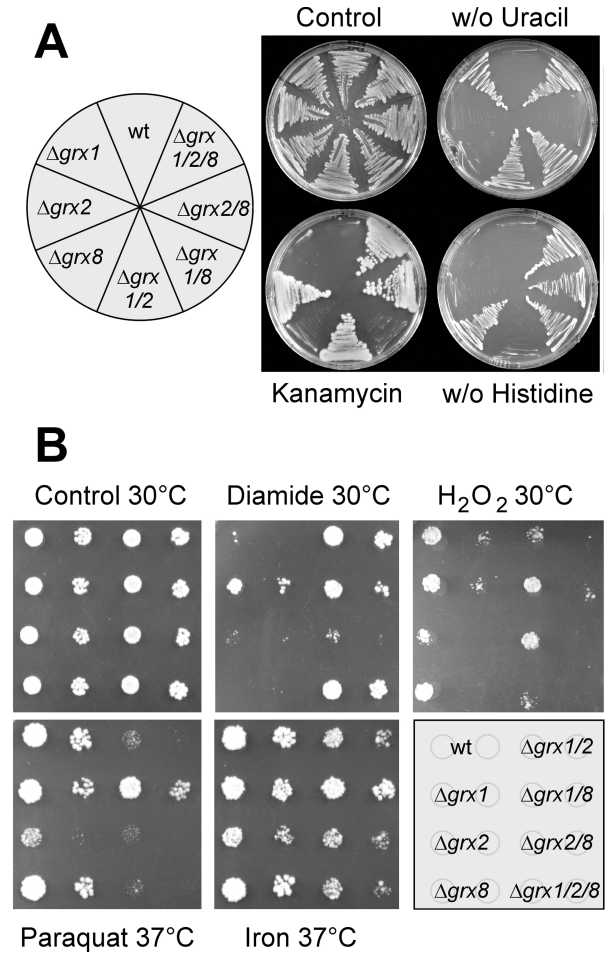

FIGURE 2: Grx8 does not contribute to the general oxidative stress resistance in yeast. (A) The *GRX1*, *GRX2*, and *GRX8* genes were replaced by *URA3*, kanamycin resistance, and *HIS3* cassettes which allow growth on uracil-deficient, kanamycin-containing or histidine-deficient plates, respectively. (B) Yeast cultures were grown to midlog phase and diluted to an OD of 0.1. 10-fold serial dilutions were dropped onto plates with synthetic growth medium containing 0.75 mM diamide or 1 mM hydrogen peroxide (upper row) or with YP medium containing 0.5 mM paraquat or 1.5 mM iron chloride (lower row). The plates were incubated at the indicated temperatures for 2 days.

proteins and could also interact with the substrate carboxylate group (*38*). At the end of α-helix 3, residue Trp^{60} probably participates in the formation of the glutathione binding site. The residue is conserved in many monothiol Grxs (Figure 3D) and could significantly alter glutathione binding and enzymatic activity of these proteins (*12*, *32*, *50*). Amino acids surrounding the potential active site cysteine residue of *Sc*Grx8 at the N-terminus of α-helix 2 are more similar to Trxs. Highest similarity at this region is found between *Sc*Grx8 and the thioredoxin-related protein of 14 kDa (Trp14 (*51*)), having a SWCPDCV motif with a tryptophan residue partially shielding the active site (Figure 3C,D). As a consequence, it is possible that the cysteine thiol groups in *Sc*Grx8 possess similar chemical properties as in Trp14 (*52*), whereas substrate binding sites and overall structures differ significantly between both proteins (Figure 3A,C). For example, a split and twisted α-helix 3 and an elongated loop preceding α-helix 2 are typical for Trp14 but are not found in *Sc*Grx8 (Figure 3A,C). We conclude that *Sc*Grx8 has a canonical Grx fold, a significantly altered substrate binding site, and a Trp14-type cysteine motif at the catalytic center.

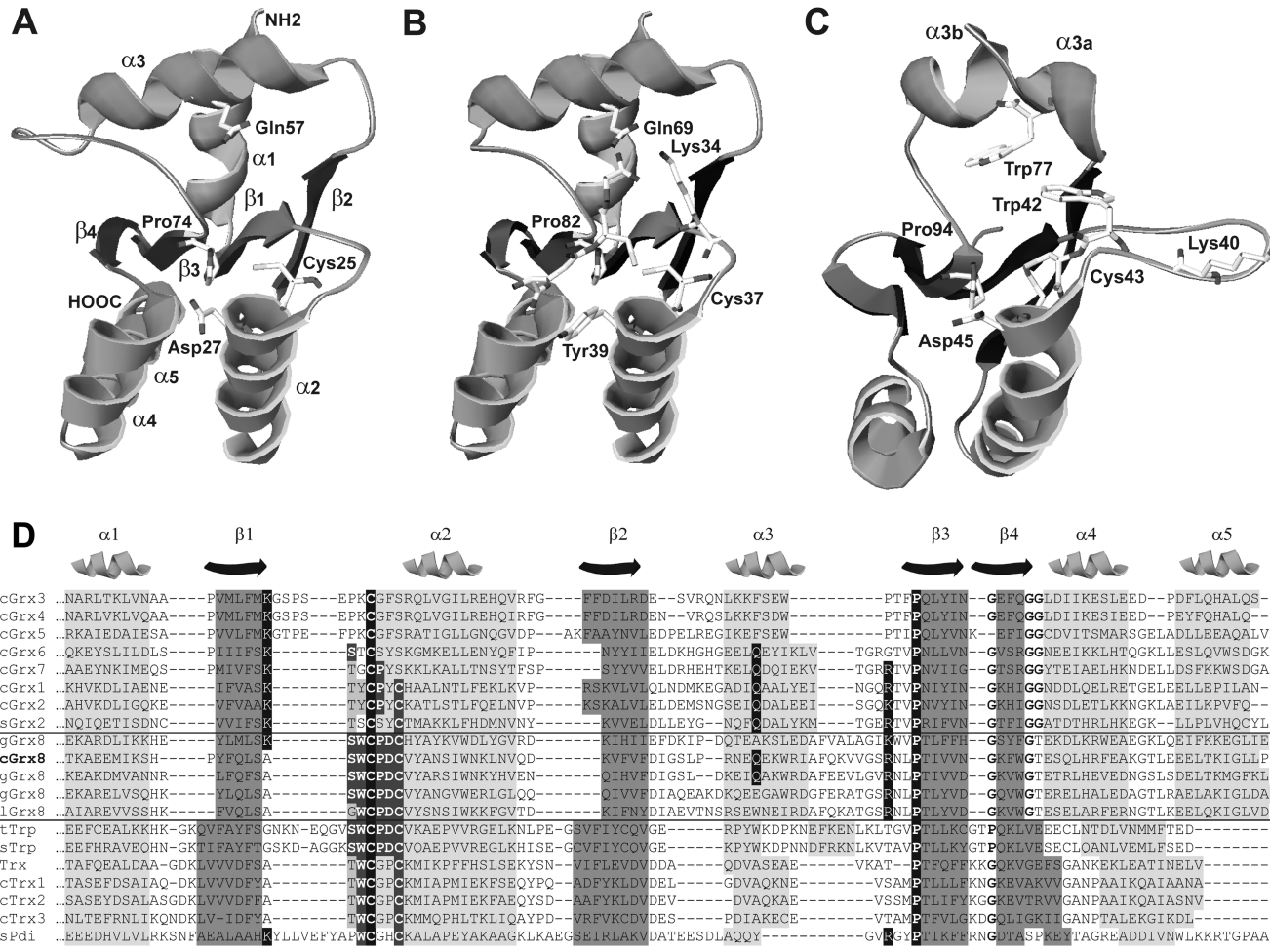

FIGURE 3: Multiple sequence alignment and molecular model of *Sc*Grx8. (A) Top view of the glutathione binding site of *Sc*Grx8. See Results for highlighted residues at the glutathione binding site. The computed force field energy of the model is −3.7 MJ/mol. (B) The model in panel A is based on the structure of human Grx2 in complex with glutathione (2FLS) (*47*). (C) The structure of oxidized human Trp14 having a SWCPDCV motif is shown for comparison (1WOU) (*51*). N-Terminal residues were removed for clarity. (D) Structural sequence alignment of (i) all eight Grx from yeast, (ii) putative homologues of Grx8 from related organisms, and (iii) further thioredoxin-fold-containing proteins. The (putative) secondary structure is indicated. *S. cerevisiae* glutaredoxins 1−8 (ScGrx1−8: gil6319814, gil6320720, gil6320303, gil6321022, gil6325198, gil6320193, gil6319488, gil6323396); uncharacterized proteins from related organisms including *Ashbya gossypii* (AgGrx8: gil45199095), *Candida glabrata* (CgGrx8: gil50288295), *Kluyveromyces lactis* (KlGrx8: gil50303875), and *Pichia guilliermondii* (PgGrx8: gil146417811); *Homo sapiens* glutaredoxin 2 isoform 1 (HsGrx2: gil21361507); *H. sapiens* Trp14 (HsTrp: gil55670733); *Xenopus tropicalis* Trp14 homologue (XtTrp: gil82653382); *H. sapiens* thioredoxin (hTrx: gil157834011); *S. cerevisiae* thioredoxins 1−3 (ScTrx1−3: gil6323072, gil6321648, gil6319925); *H. sapiens* protein disulfide isomerase (HsPdi: gil2098329).

Cloning, Expression, and Purification. Recombinant N-terminally His-tagged *Sc*Grx8 was successfully expressed in *E. coli* and purified by Ni-NTA affinity chromatography, yielding approximately 2.5 μmol (35 mg) of pure protein/L of culture. The calculated molecular mass of 13700 Da was confirmed by mass spectrometry (13697 and 13699 Da for oxidized and reduced protein, respectively; data not shown). *Sc*Grx8 slowly started to precipitate after several days of storage at 4 °C. Eluates of *Sc*Grx8 were colorless and did not contain significant amounts of calcium, magnesium, arsenic, molybdenum, manganese, iron, cobalt, nickel, copper, or zinc. In contrast to *Sc*Grx7, the protein is monomeric as revealed by gel filtration chromatography and reducing/nonreducing SDS−PAGE (Figure 4). Our previous studies on *Sc*Grx7 purified from *E. coli* revealed two major protein subpopulations. The less abundant protein form showed a mass shift of 1090 ± 14 Da in comparison with unmodified *Sc*Grx7 (20241 Da), but a putative secondary modification could not be identified (*12*). The exact mass shift was now determined to be 1080 ± 1 Da. Both subpopulations of *Sc*Grx7 were partially glutathionylated when purified from *E. coli* as indicated by a mass shift of 305 Da (Supporting Information Figure S1). Inserting an additional stop codon, we were furthermore able to produce homogeneous unmodified *Sc*Grx7 (Supporting Information Figure S2A). These protein preparations were used for the enzymatic analyses described below.

ScGrx8 Has Low Dithiol-Dependent Activity in the HEDS Assay. An initial analysis of *Sc*Grx8 in the HEDS assay revealed that micromolar protein concentrations were required to measure a significant activity (Figure 5A). *Sc*Grx7 (25 nM) served as a positive control confirming the functionality of the assay. The consumption of NADPH due to an oxidase activity and other background reactions was subtracted in all assays using a reference cuvette without a Grx. Using 25 μM *Sc*Grx8 and millimolar substrate concentrations, the GR-dependent regeneration of GSH became rate-limiting when assays were performed with less than 1 unit/mL GR (Figure 5B). In similarity to *Sc*Grx7 (*12*), the activity of *Sc*Grx8 was higher, and after mixing an initial lag phase

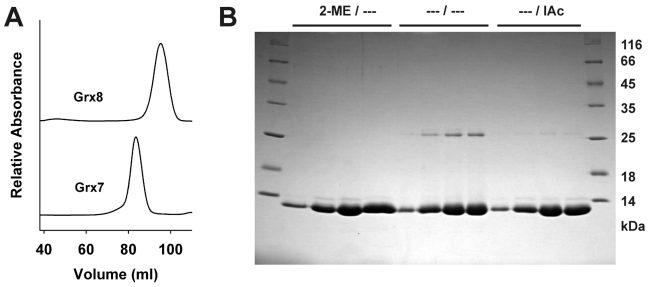

FIGURE 4: *Sc*Grx8 is monomeric and does not form covalently linked dimers. (A) Gel filtration analysis of freshly purified recombinant *Sc*Grx8 with a theoretical molecular mass of 13.7 kDa. The apparent molecular mass of *Sc*Grx8 determined from the upper chromatogram at 280 nm was 14.9 kDa. Freshly purified recombinant *Sc*Grx7 (theoretical molecular mass of 20.2 kDa) eluted as a dimer with an apparent molecular mass of 42.2 kDa and is shown for comparison in the lower chromatogram. (B) SDS−PAGE analysis of *Sc*Grx8 purified by gel filtration. Protein-containing fractions were boiled in sample buffer with or without 2-mercaptoethanol (2-ME) before SDS−PAGE. In order to exclude a boiling-induced formation of disulfide bonds, a third sample was pretreated with 2 mM iodoacetamide (IAc) to block free thiol groups.

was less pronounced, when the assay was started with Grx instead of HEDS. Both glutathione:HEDS and glutathione:GSSCys thioltransferase activities of *Sc*Grx8 were rather small (Figure 5C). To exclude an activity due to trace amounts of *E. coli* Grxs that were undetectable in Coomassie-stained gels, we purified and analyzed recombinant *Sc*Grx8^{C25S} and *Sc*Grx8^{C28S} analogously. No enzymatic activity was detectable for both proteins (data not shown). Cysteine residues in a SWCPDCV motif can form an intramolecular disulfide bond as indicated by the crystal structure of human Trp14 (*51*). To ascertain that the consumption of NADPH in the assay was not due to reduction of highly concentrated oxidized enzyme (e.g., Grx containing an intramolecular disulfide bond or a glutathionylated cysteine residue), we performed several controls (Figure 5D) and determined the redox status of freshly purified and aged *Sc*Grx8 by DTNB assays (Figure 6): No significant amounts of NADPH were oxidized in the absence of HEDS, and the measured activity clearly depended on the presence of all assay components (Figure 5D). Compared to $NaBH_4$-reduced protein, about 90% of the cysteine residues in freshly purified *Sc*Grx8 were reduced and unmodified (Figure 6A). DTNB accessibility of SH groups was very similar for native and denatured protein. Aerobic storage of protein samples led to a slow increase of oxidized protein over time (Figure 6B). Thus, using 25 μM freshly purified enzyme in the assay, oxidized protein could theoretically have caused an estimated ΔAbs_{340nm} of ~0.015, which is smaller than the observed decrease in absorbance as seen in Figure 5C. Nevertheless, in all of the following HEDS assays we determined kinetic parameters with $NaBH_4$-reduced *Sc*Grx8.

Using 2 mM GSH and variable concentrations of HEDS, kinetic data could be approximately fitted according to Michaelis−Menten theory, and a K_m^{app} value of 0.5 mM and a k_{cat}^{app} value of 0.019 s^{-1} were estimated (Figure 5E). Please note that the actual substrate is formed during a preincubation period (Figure 1) and that initial concentrations of GSH and HEDS are indicated (see Discussion). Varying the concentration of GSH at 0.74 mM HEDS, a rather sigmoidal curve was obtained with an inflection point around 1 mM GSH

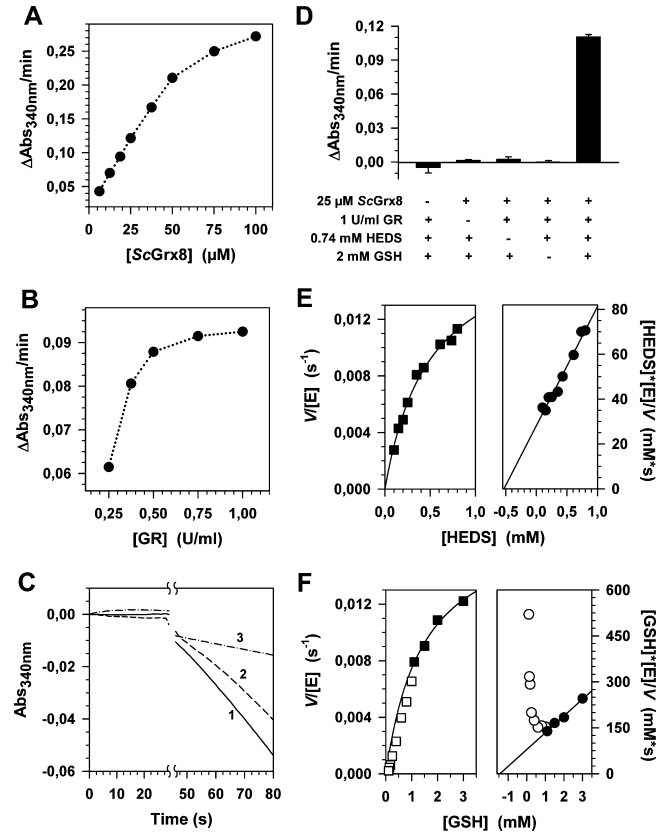

FIGURE 5: *Sc*Grx8 has slight activity in the HEDS assay. The oxidation of NADPH at 25 °C was followed spectrophotometrically at 340 nm in a coupled enzymatic assay (see Materials and Methods and Figure 1 for further details). (A) Reaction velocities with 0.74 mM HEDS and 2 mM GSH were proportional to the concentration of *Sc*Grx8 at an enzyme concentration ≤50 μM. (B) Using 25 μM *Sc*Grx8, a GR concentration below 1 unit/mL became rate-limiting at high substrate concentrations (0.74 mM HEDS and 2 mM GSH). (C) Representative time courses of three single measurements: A baseline was recorded before the assay was started by the addition of either enzyme (curve 1) or disulfide (curves 2 and 3). Curves 1 and 2 were obtained with 0.74 mM HEDS and 1 mM GSH. Curve 3 resulted from a measurement with 0.4 mM GSH and 0.1 mM GSSCys. (D) Consumption of NADPH in the assay depended on HEDS and GSH and was not caused by oxidized *Sc*Grx8. Components that were varied in the sample cuvette are indicated. The sample without *Sc*Grx8 contained elution buffer that was analogously pretreated with $NaBH_4$ as a control. (E) HEDS-dependent activity of *Sc*Grx8 followed Michaelis−Menten kinetics. A direct plot (left side) and a Hanes plot (right side) from a representative experiment with samples containing 25 μM $NaBH_4$-reduced *Sc*Grx8, 2 mM GSH, and the indicated concentrations of HEDS are shown. (F) The GSH-dependent activity of *Sc*Grx8 did not follow typical Michaelis−Menten kinetics. A direct plot (left side) and a Hanes plot (right side) from a representative experiment with samples containing 25 μM $NaBH_4$-reduced *Sc*Grx8, 0.74 mM HEDS, and the indicated concentrations of GSH are shown. Only data at high GSH concentrations (closed symbols) were used for regression analysis.

(Figure 5F) which could be in the physiological concentration range. This result is in clear contrast to our previous studies on *Sc*Grx7 (see Figure 8A in ref *12*). Positive subunit cooperativity is unlikely to have caused the sigmoidal curve since *Sc*Grx8 was found to be exclusively monomeric even when the protein was purified and subsequently analyzed by gel filtration in the presence of 2 mM GSH (data not shown). Further possible causes are (i) deviation from Michaelis−Menten assay conditions at low GSH and high *Sc*Grx8 concentrations or (ii) kinetic cooperativity due to

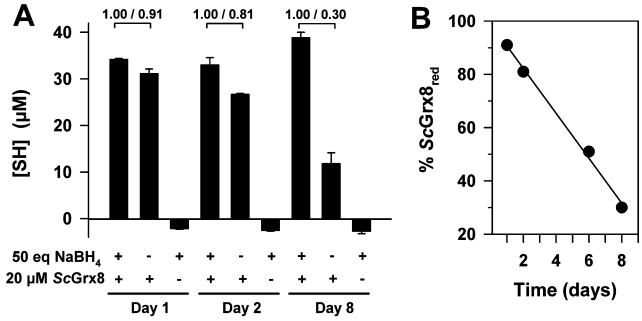

FIGURE 6: Freshly purified *Sc*Grx8 is mainly reduced and oxidizes slowly. (A) The concentration of unmodified thiol groups was analyzed with DTNB. Solutions containing 0.16 mM freshly purified or aged *Sc*Grx8 were pretreated with or without 50 equiv of $NaBH_4$ for 1.5 h at room temperature. A negative control containing $NaBH_4$ in elution buffer was always incubated in parallel. Afterward, samples were diluted in the DTNB assay, resulting in a theoretical concentration of cysteine thiol groups of ~40 μM. Excess $NaBH_4$ was obviously degraded and did not reduce DTNB in the assay. Ratios between thiol concentrations of samples with and without $NaBH_4$ are indicated. (B) The ratios determined in (A) were plotted versus time, yielding apparent zero-order kinetics for the oxidation of *Sc*Grx8 ($V = -d[ScGrx8_{red}]/dt = k_0^{app} \approx 0.08\%$ per day at 4 °C).

slow conformational changes (see Discussion). Estimated values for K_m^{app} and k_{cat}^{app} with 0.74 mM HEDS and higher concentrations of GSH were ~1.5 mM and 0.018 s^{-1}, respectively (Figure 5F). K_m^{app} values determined from Figure 5E,F are in the same concentration range as for *Sc*Grx7, whereas values for k_{cat}^{app} are 3 orders of magnitude smaller (*12*). To answer the question of which part in the HEDS reaction is much slower for *Sc*Grx8 than for *Sc*Grx7, we performed the following experiments.

ScGrx8 Disulfide Is Slowly Reduced by GSH. We first asked whether *Sc*Grx8 disulfide itself is a good substrate for the GR/GSH system (steps 7−9 in Figure 1). Reversibly oxidized *Sc*Grx8 with a purity ≥95% was obtained after treatment with diamide as revealed by DTNB assays. The repurified protein did not contain detectable amounts of intermolecular disulfide bonds (Figure 7A). Varying the initial concentration of *Sc*Grx8 at 2 mM GSH, reaction velocity 10 s after mixing showed a linear correlation (Figure 7B). The actual concentration of *Sc*Grx8 disulfide was calculated from the consumption of NADPH and plotted versus time, yielding exponential curves (Figure 7C). Based on these calculations, reduction of *Sc*Grx8(S_2) by GSH followed apparent first-order kinetics ($V = k^{app}[ScGrx8(S_2)]$) with a constant value for k^{app} of ~0.045 s^{-1} (Figure 7D). GSH dependency of k^{app} is summarized in Figure 7E−H: Using 15 μM *Sc*Grx8(S_2) and varying the concentration of GSH, the reaction velocity showed a hyperbolic correlation (Figure 7E). Again, the actual concentration of *Sc*Grx8 disulfide was calculated from the consumption of NADPH and plotted versus time (Figure 7F), resulting in apparent first-order kinetics (Figure 7G). Please note that k^{app} (the negative slope in the plot) increased for increasing GSH concentrations (Figure 7G). Analysis of the slopes determined from Figure 7G suggests a rather complex correlation between k^{app} and the concentration of GSH (Figure 7H): Below 1 mM GSH the quotient k^{app}/[GSH] increases with increasing concentration of GSH, whereas above 1 mM GSH the quotient decreases. Hypothetical rate-limiting steps during the reduction of *Sc*Grx8(S_2) by two molecules of GSH are summarized in Figure 7I. Such a step might be the following: (i) Reaction of a ternary complex ($k^{app} = k_1[GSH]^2$); however, plotting k^{app} versus $[GSH]^2$ did not yield a straight line and a ternary complex is not in agreement with the scheme shown in Figure 1. (ii) Reaction of a binary complex either between GSH and *Sc*Grx8(S_2) ($k^{app} = k_2[GSH]$) or between GSH and the mixed disulfide ($k^{app} = k_3[GSH]$); however, plotting k^{app} versus [GSH] a sigmoidal curve was obtained (data not shown). The kinetic law for the reduction of *Sc*Grx8(S_2) is therefore more complex, most likely due to (iii) rate-influencing substrate binding kinetics and/or GSH-dependent conformational changes.

Reduction of Glutathionylated ScGrx7 and ScGrx8 by GSH Differs Significantly. Reduction of glutathionylated *Sc*Grx8 by the GR/GSH system might be much slower than for other Grxs, resulting in a decreased activity in the HEDS assay. To test this hypothesis, we compared reduction of *Sc*Grx7-SSG and *Sc*Grx8^{C28S}-SSG by GSH. Efficient glutathionylation of both proteins (>95% for *Sc*Grx7 and *Sc*Grx8^{C28S}) after incubation with GSSG was confirmed by DTNB assays (data not shown) and mass spectrometry (Supporting Information Figure S2A−D). We chose *Sc*Grx8^{C28S} instead of wild-type enzyme because incubation of the latter with GSSG resulted in unmodified *Sc*Grx8 disulfide (data not shown). The single cysteine residue in *Sc*Grx8^{C25S} could not be glutathionylated (Supporting Information Figure S2E), which is in agreement with the catalytic mechanism shown in Figure 1. Varying the initial concentration of *Sc*Grx7-SSG at 2 mM GSH, reaction velocities 10 s after mixing were slightly higher than for *Sc*Grx8^{C28S}-SSG (Figure 8A,B). The actual concentration of *Sc*Grx8^{C28S}-SSG and *Sc*Grx7-SSG in the assay was calculated from the consumption of NADPH, plotted versus time (Figure 8C,D), and used to determine apparent first-order kinetic constants ($V = k^{app}$[Grx-SSG)]) (Figure 8E,F). For *Sc*Grx8^{C28S}-SSG a constant k^{app} of 0.029 s^{-1} was estimated. Reduction of *Sc*Grx7-SSG was about five times faster (0.15 ± 0.02 s^{-1}) (Figure 8F), and accordingly far more reactant was consumed right after mixing (Figure 8D). Varying the initial concentration of GSH between 0.11 and 4 mM at 15 μM Grx-SSG, reaction velocities 10 s after mixing were variable for *Sc*Grx8^{C28S}-SSG and rather constant for *Sc*Grx7-SSG (Figure 8G,H). Both reductions followed apparent first-order kinetics as indicated by the straight lines in Figure 8K,L. However, velocities significantly increased at higher GSH concentrations for *Sc*Grx8^{C28S}-SSG (Figure 8I,K) whereas kinetics did not depend on GSH for *Sc*Grx7-SSG (Figure 8J,L). Thus, under the chosen conditions, kinetic law for the reduction of *Sc*Grx7 by GSH is $V = (0.15\ s^{-1})$[*Sc*Grx7-SSG]. The kinetic law for the reduction *Sc*Grx8^{C28S}-SSG could not be determined, again due to a more complex dependency between k^{app} and [GSH]. In conclusion, at a low glutathione concentration the reductive half-reaction of *Sc*Grx8 was much slower than for *Sc*Grx7. However, reduction of *Sc*Grx^{C28S}-SSG became significantly faster at high glutathione concentrations whereas the velocity for the reduction of *Sc*Grx7-SSG was unchanged.

ScGrx8 Has Low Activity in the Insulin Assay. Most Trxs are far more efficient in the reduction of insulin disulfide bonds than Grxs (*19*, *21*, *29*, *31*, *52*). Due to its unusual structural properties (Figure 3), we tested *Sc*Grx8 for a Trx-like activity in a turbidimetric insulin assay (Figure 9). Trx from *E. coli* served as a positive control (Figure 9A). A low

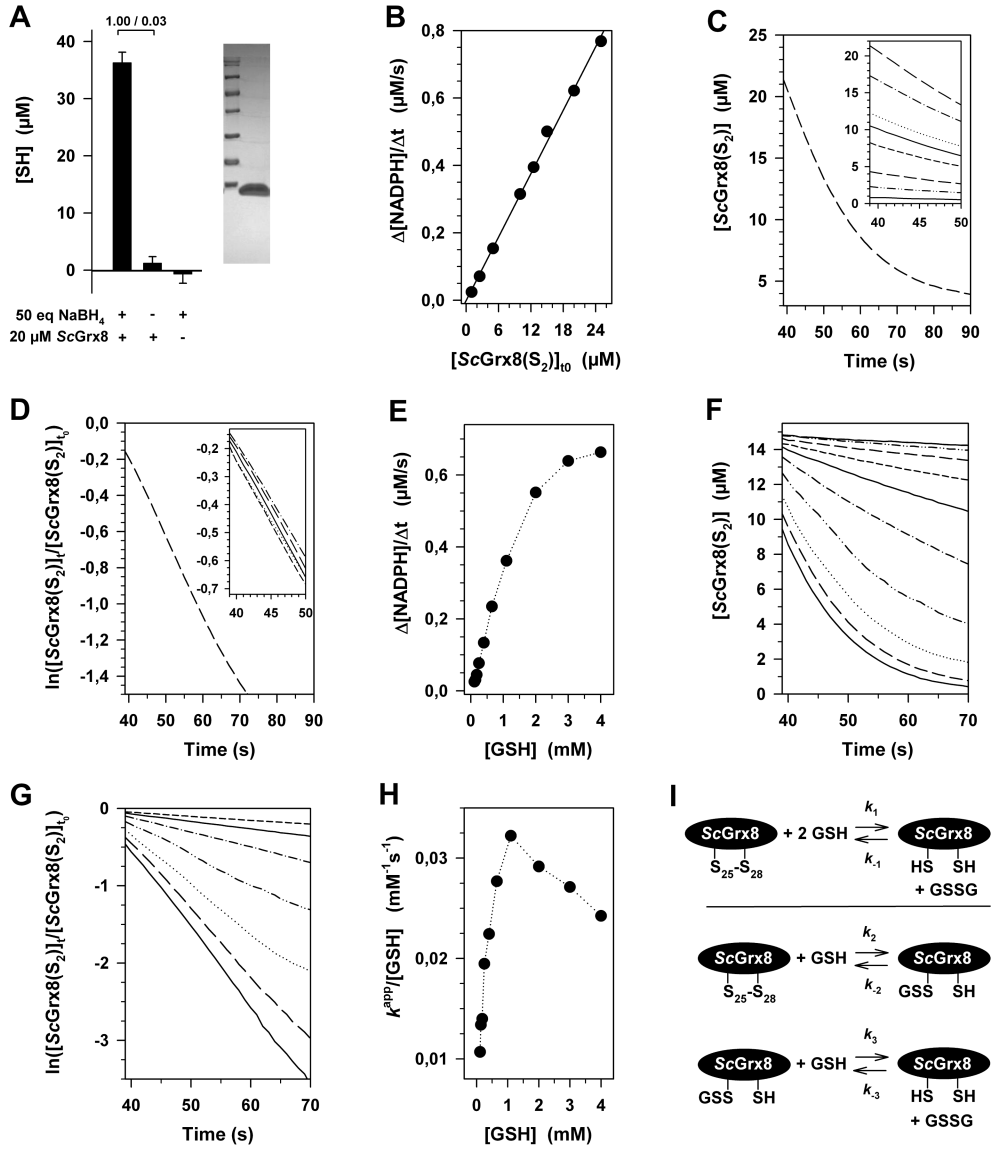

FIGURE 7: *Sc*Grx8 disulfide is a poor substrate of the GR/GSH system. Freshly purified protein was oxidized with diamide and analyzed as a substrate for the GR/GSH system. (A) Reversible intramolecular disulfide formation after diamide treatment was confirmed by DTNB assays (see Figure 6 for further details) and nonreducing SDS−PAGE. Results from assays containing 1 unit/mL yeast GR, 0.1 mM NADPH, 2 mM GSH, and 1−25 μM *Sc*Grx8(S_2) at 25 °C are shown in panels B−D. (B) Reaction velocities 10 s after mixing were plotted versus the initial concentration of *Sc*Grx8(S_2), yielding a linear dependency. (C) The actual concentration of *Sc*Grx8 disulfide during the reaction was calculated from the consumption of NADPH and plotted versus time. (D) Reduction of *Sc*Grx8(S_2) followed apparent first-order kinetics. The value for k^{app} of ~0.045 s^{-1} determined from the negative slope of the straight lines was independent of the *Sc*Grx8 concentration. Alternatively, the concentration of GSH (0.1−4 mM) was varied in assays containing initially 15 μM *Sc*Grx8(S_2). Results from these experiments are shown in panels E−H. (E) Reaction velocities 10 s after mixing were plotted versus the concentration of GSH, yielding a hyperbolic curve. (F) The actual concentration of *Sc*Grx8(S_2) during the reaction was calculated from the consumption of NADPH and plotted versus time. (G) Reduction of *Sc*Grx8(S_2) followed apparent first-order kinetics at all GSH concentrations tested. (H) The correlation between k^{app} obtained from panel G and the applied concentration of GSH is complex and does not suggest simple first- or second-order kinetics. (I) Potential rate-limiting steps during GSH-dependent reduction of *Sc*Grx8(S_2).

but concentration-dependent activity was detected for *Sc*Grx8 (Figure 9B), and insulin reduction was more efficient than in the imidazole-containing negative controls. However, considering (i) the protein concentrations, (ii) the time points when the turbidity started to increase, and (iii) the maximum slopes (ΔAbs/min) of the plots, the activity of *Sc*Grx8 was much lower than for *Ec*Trx. The results are very similar to an insulin assay with Trx and Grx from *P. falciparum* (*29*).

Yeast TrxR Does Not Reduce Oxidized ScGrx8 or Glutathionylated ScGrx7. *Ec*Grx4 and human mitochondrial Grx have been previously shown to accept electrons from TrxR (*25*, *33*). In addition, since the active site motif of *Sc*Grx8 shares more similarity with thioredoxins, we tested *Sc*Grx8(S_2) as substrate of yeast TrxR (see Materials and Methods). No significant activity was observed. This was also the case for *Sc*Grx7-SSG (data not shown).

DISCUSSION

Grx8, a Novel Dithiol Glutaredoxin of Baker's Yeast. Extensive blast searches on the yeast genome identified eight genes coding for glutaredoxin-like proteins. Seven of these, the two dithiol glutaredoxins Grx1 and Grx2 and five monothiol glutaredoxins Grx3 to Grx7, were characterized previously. Grxs play a pivotal role in cellular oxidative stress response. Nevertheless, with the exception of Grx5, which

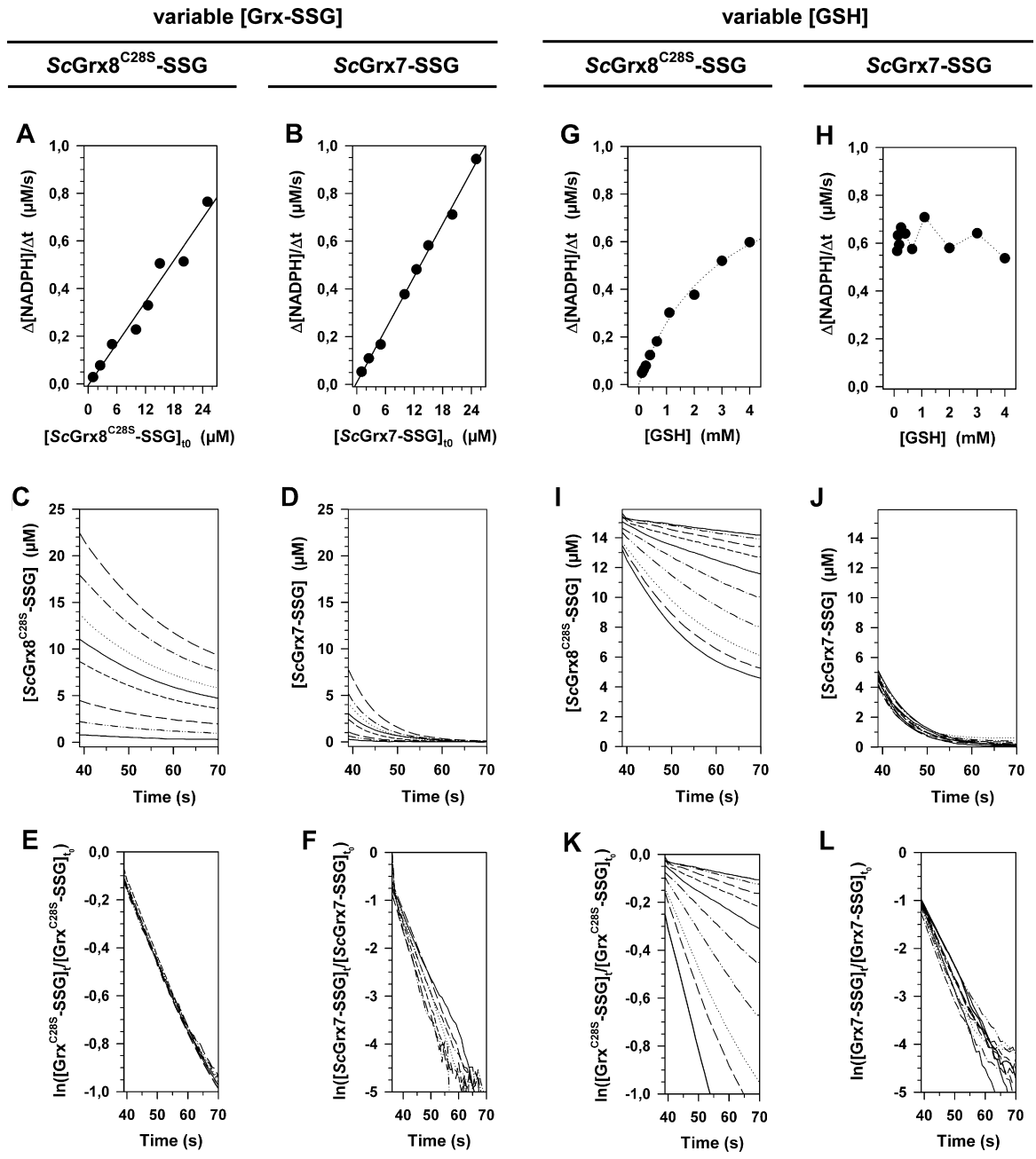

FIGURE 8: Reduction of glutathionylated *Sc*Grx7 and *Sc*Grx8^{C28S} by the GR/GSH system. Freshly purified protein was oxidized with GSSG (Supporting Information Figure S2) and analyzed as a substrate for the GR/GSH system. Assays in panels A−F were performed with 1 unit/mL yeast GR, 0.1 mM NADPH, 2 mM GSH, and 1−25 μM Grx-SSG at 25 °C. (A) Reaction velocities 10 s after mixing were plotted versus the initial concentration of *Sc*Grx8^{C28S}-SSG, revealing a linear dependency. (B) Analogous experiments with *Sc*Grx7-SSG led to similar results with slightly higher reaction velocities. The actual concentrations of *Sc*Grx8^{C28S}-SSG (C) and *Sc*Grx7-SSG (D) were calculated from the consumption of NADPH and plotted versus time. Reduction of *Sc*Grx8^{C28S}-SSG (E) and *Sc*Grx7-SSG (F) followed apparent first-order kinetics. Negative slopes of the straight lines were used to estimate values for k^{app}. In both cases values were independent of the protein concentration. Alternatively, the concentration of GSH (0.1−4 mM) was varied in assays containing 15 μM Grx-SSG. Results from these experiments are shown in panels G−L. Reaction velocities 10 ss after mixing were plotted versus the concentration of GSH, yielding a hyperbolic curve for *Sc*Grx8^{C28S}-SSG (G) and a rather constant value for *Sc*Grx7-SSG (H). The actual concentrations of *Sc*Grx8^{C28S}-SSG (I) and *Sc*Grx7-SSG (J) were calculated from the consumption of NADPH and plotted versus time. Both reactions followed apparent first-order kinetics as indicated by the straight lines; however, k^{app} values for *Sc*Grx8^{C28S}-SSG increased with increasing concentration of GSH (K) whereas k^{app} was rather constant for *Sc*Grx7-SSG (L).

plays a specific role in mitochondrial iron−sulfur cluster biogenesis (*8*, *56*), individual or combined deletions of glutaredoxin genes only cause mild growth defects even under oxidative growth conditions (*6*) (Figure 2). This is due to the functional overlap of the glutaredoxin activity with that of Trxs, of which numerous isoforms are ubiquitously present in the different compartments of the cell. Deletion of *GRX8* did not increase the growth defects observed for mutants of the other dithiol Grxs. This excludes that Grx8 is simply a backup for Grx1 and Grx2. Also, the primary sequence of Grx8 is rather unique, which might point to a specialization of this enzyme.

Is ScGrx8 Really a Glutaredoxin? Considering the low or even absent catalytic activity of *Sc*Grx8 and most monothiol Grxs, one might argue that several of these proteins are not glutathione-dependent. Moreover, the absence of a detectable

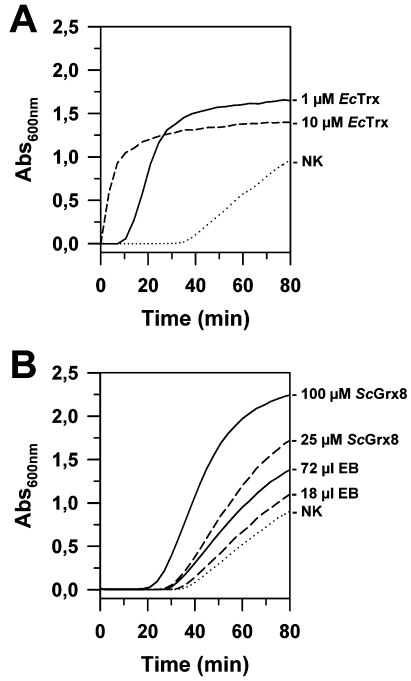

FIGURE 9: *Sc*Grx8 has low activity in the insulin assay. The reduction of insulin by 1 mM DTT in the presence and absence of *Ec*Trx or *Sc*Grx8 was monitored in a turbidimetric assay at 600 nm (see Materials and Methods for further details). (A) Results from assays containing 1 or 10 μM *Ec*Trx and a negative control without *Ec*Trx (NK) are shown. (B) Results from assays containing 25 or 100 μM *Sc*Grx8 and a negative control without *Sc*Grx8 are shown. The same volume of elution buffer (EB) containing 125 mM imidazole was added to further negative controls for comparison (18 or 72 μL of buffer was added to a final assay volume of 1 mL).

growth defect under oxidative stress conditions might challenge the idea of *Sc*Grx8 being a significant physiological reductant. Nevertheless, three aspects support a glutathione-dependent activity of *Sc*Grx8: (i) Molecular models suggest that some glutathione binding residues are present in *Sc*Grx8, although the active site structure is significantly different from other Grxs, and the cysteine motif has more similarities with Trxs (Figure 3). (ii) *Sc*Grx8 has a measurable activity in the HEDS assay, and K_m^{app} values are comparable to other Grxs (Figure 5). (iii) Reduction of oxidized *Sc*Grx8 by GSH is not a simple chemical reaction with second-order kinetics but shows half-saturation in the physiological lower millimolar concentration range (Figures 7E and 8G). We conclude that the classification of *Sc*Grx8 as a glutaredoxin is justified. Thus, regarding absent or slight catalytic activity of Grxs, either the oxidative or the reductive half-reaction could be too slow or could not occur for thermodynamic reasons (see hypotheses 1 and 2 below).

Further Data Confirm a Ping-Pong Mechanism for ScGrx7. On the basis of enzyme kinetic patterns and a widely accepted catalytic mechanism for dithiol Grxs, we previously postulated that catalysis by *Sc*Grx7 also involves a glutathionylated enzyme as an intermediate (*12*). Now three more experimental results support the model: (i) *Sc*Grx7 can be efficiently glutathionylated *in vitro*, (ii) the recombinant protein is also partially glutathionylated in *E. coli*, and (iii) *Sc*Grx7-SSG is fully active in the HEDS assay (data not shown). We conclude that *Sc*Grx7-mediated (de)glutathionylation of substrates efficiently occurs via steps 2 and 3 as shown in Figure 1 with the modification that *Sc*Grx7 is a monothiol Grx.

Activity of ScGrx8 in the HEDS Assay Is Based on a Dithiol Mechanism. Grx(S_2) formation is currently considered to be more or less irrelevant during reduction of glutathionylated substrates (for example, see the catalytic mechanism summarized in ref *4*). However, reversible intramolecular disulfide bond formation (step 7 in Figure 1) was always included as a possible side reaction in the original publications on the catalytic mechanism of dithiol Grxs (*35*−*38*, *53*). Kinetic studies on human Grx indeed showed that such a side reaction can occur to a significant extent, leading to a decreased overall activity (see Figure 1 in ref *38*). Mutant dithiol Grxs (*30*, *35*, *38*, *53*) and the monothiol glutaredoxins *Sc*Grx6 and *Sc*Grx7 (*12*) did not require a second cysteine residue for the glutathione-dependent reduction of HEDS. Lack of activity for *Sc*Grx8^{C25S} and *Sc*Grx8^{C28S} is therefore surprising. Our results suggest that the slight activity of wild-type enzyme is exclusively based on a dithiol mechanism in contrast to any other Grx studied so far.

How can step 7 of the mechanism shown in Figure 1 become a prerequisite for the reduction of GSSEtOH? Either the model is too simple or *Sc*Grx8 gets directly oxidized by HEDS (steps 5 and 6 in Figure 1 with HEDS replacing R″(S_2)). A direct oxidation of Grx by HEDS could also explain why most monothiol Grxs are inactive in the assay: After rapid formation of Grx-SSEtOH, reduction of this protein species might be slow, leading to inactivated enzyme. In contrast to monothiol Grxs, dithiol Grxs might become reactivated due to the second cysteine residue liberating 2-ME. However, four aspects speak against a direct reaction between Grx and HEDS: (i) The monothiol glutaredoxin *Pf*Glp1-N (*29*, *32*) also has no significant activity in the GSH: GSSCys thioltransferase assay (unpublished results). Please note that this assay lacks a potential inactivating non-glutathione disulfide. (ii) The activity of *Sc*Grx8 in this assay is also low (Figure 5C). (iii) Values for K_m^{app} of *Sc*Grx8 are very similar to other Grxs (*12*, *21*, *23*, *25*) and may be interpreted as comparable substrate affinities for GSSEtOH. (iv) A lag phase is observed for human Grx (*23*), *Sc*Grx7 (*12*), and *Sc*Grx8 (Figure 5C) when the assay is started with HEDS, probably because the substrate GSSEtOH has to be formed first (step 1 in Figure 1). We conclude that the mechanism shown in Figure 1 is too simple to explain the data obtained for *Sc*Grx8.

Hypothesis 1. The Oxidative Half-Reaction Is Rate-Limiting in the HEDS Assay. Step 2 in Figure 1 could limit catalytic turnover of slightly active or inactive Grxs because of an excessively high (i) activation energy, (ii) redox potential, (iii) thiol pK_a value, and/or (iv) steric hindrance. As a result the steady-state concentration of Grx-SSG is lowered, and $k_{cat}^{app} = V/[E]_0$ is reduced. From causes i−iv, insufficient thiolate formation for nucleophilic attack at pH 8 is the most unlikely one. First, the more N-terminal cysteine residue in Trp14, containing the same cysteine motif as *Sc*Grx8 (Figure 3D), has a pK_a^{app} of 6.1 (*52*). Second, two different monothiol Grxs were shown to have a cysteine thiol pK_a^{app} of approximately 5 (*10*, *32*). Thus, active site cysteine residues of these Grxs are deprotonated both in the assay and *in vivo*. A very high redox potential of the Grx_{red}/Grx-SSG couple for all inactive Grxs is also questionable because several were shown to react with GSSG, resulting in

efficiently glutathionylated protein species (Figures S1 and S2) (*10*, *32*, *33*). (The high redox potential of −175 mV for inactive *Sc*Grx5 reflects the couple Grx5$(SH)_2$/Grx5(S_2) with a disulfide bond between residue 60 at the active site and residue 117 before α-helix 4 (*10*)). In summary, if hypothesis 1 is correct, steric hindrance and/or high activation energy are (is) the most likely reason(s) for the reduced activity of *Sc*Grx8 and inactive monothiol Grxs.

Hypothesis 2. The Reductive Half-Reaction Is Rate-Limiting in the HEDS Assay. The reductive half-reaction (step 3 in Figure 1), starting with the nucleophilic attack by the glutathionyl thiolate species, has been demonstrated to be rate-limiting for human dithiol Grx mainly due to the high thiol pK_a value of GSH (*37*). GSH was also shown to be a poor reductant for several monothiol Grxs (*10*, *31*, *33*). Indeed, values for (i) k_{cat}^{app} of *Sc*Grx8 in the HEDS assay (0.018 s^{-1}, Figure 5F), (ii) k^{app} for the reduction of *Sc*Grx8 disulfide (0.045 s^{-1}, Figure 7D), and (iii) k^{app} for the reduction of *Sc*Grx8^{C28S}-SSG (0.029 s^{-1}, Figure 8E) are quite similar, supporting hypothesis 2. Since k_{cat}^{app} is smaller than the k^{app} values, the reductive half-reaction might be inhibited during turnover (or another process is even slightly slower). The fact that reduction of *Sc*Grx8(S_2) (steps 7 and 8 in Figure 1) is faster than reduction of *Sc*Grx8^{C28S}-SSG suggests that step 7 occurs more rapidly than step 8 and that the mutation at the active site has a modest negative influence. In conclusion, we favor hypothesis 2 over hypothesis 1 for *Sc*Grx8 but do not rule out activation energies or steric hindrance as important limiting factors for selected Grxs (see below).

A comparison of the reductive half-reactions of *Sc*Grx7 and *Sc*Grx8^{C28S} reveals two main differences between both proteins: (i) Deglutathionylation of *Sc*Grx8^{C28S} is about five times slower and, under the chosen assay conditions, (ii) depends on the GSH concentration in contrast to deglutathionylation of *Sc*Grx7 (Figure 8). Surprisingly, the kinetic constant for the regeneration of *Sc*Grx7 ($k = 0.15$ s^{-1}) is almost 3 orders of magnitude smaller than the k_{cat} value ($k_{cat}^{app} = 76$ s^{-1} and $k_{cat} = 133$ s^{-1} in the HEDS and GSSCys thioltransferase assay, respectively (*12*)). Since we confirmed that *Sc*Grx7-SSG had the same activity in the HEDS assay as unmodified protein (starting the assay with *Sc*Grx7-SSG without preincubation of the enzyme in the presence of GSH; data not shown), the only difference between the experiments is the presence or absence of HEDS/GSSEtOH and the Grx concentration. How can the overall reaction for *Sc*Grx7 be much faster than the reductive half-reaction? To solve this discrepancy, we hypothesize that there are alternative protein conformations resulting in different enzymatic activities (see below).

Conformational Changes as a General Catalysis-Controlling Factor in Grxs and Trxs? Several results also point to conformational changes for *Sc*Grx8. Under aerobic conditions dithiol Grxs are often purified as protein disulfides. Autoxidation of *Sc*Grx8$(SH)_2$ (Figure 6B), however, is very slow, despite good reducing capacity with GSSG, and does not depend on the protein concentration. This indicates that the thiol groups are quite protected. The nonlinear and nonhyperbolic [GSH] dependency of k_{cat}^{app} and k^{app} (Figures 5F, 7G,H, and 8K) furthermore suggests that an interaction with glutathione results in structural changes. In the absence of the physiological substrate (e.g., during storage but also in the HEDS assay) most *Sc*Grx8 molecules might be in an inactive and protected conformation resulting in the small value for k_{cat}^{app}. Efficient activation might only occur upon binding of the physiological substrate. An induced fit during the oxidative or reductive half-reaction might also explain why Trp14 is mostly inactive in several redox assays despite its low redox potential of −257 mV (*52*). Conformational changes upon glutathionylation were also shown for *E. coli* Grx3 (*54*) and have been suggested for the monothiol glutaredoxin *Ec*Grx4 (*50*). A recent study on *E. coli* Trx proposed that the formation of a correct S_N2 geometry during substrate reduction can be rate-limiting (*55*). Thus, slight conformational changes in the oxidoreductase and/or the disulfide substrate can be as important as macroscopic redox potentials and pK_a values, and we are just at the beginning of understanding these aspects for selected Grxs and Trxs. Considering the low reactivity of Trp14 and *Sc*Grx8, we hypothesize that the SWCPDCV motif could be the result of a convergent evolution leading to constraints of the active site that might be suited to control enzyme reactivity and to increase substrate specificity.

Refined Model of the Catalytic Mechanism. Which glutathione interaction are we looking at? Numerous enzymatic and structural studies on Grxs have significantly improved our understanding of these proteins during the last 3 decades. However, a detailed model of the catalytic mechanism going beyond the scheme shown in Figure 1 is still missing. Here, catalytic concepts named the "glutathione scaffold model", the "glutathione activator model", and the "cysteine resolving model" are presented. The putative models are based on widely accepted thiol chemistry and discriminate between the protein area interacting with the glutathione moiety of the disulfide substrate (Figure 10A) and the protein area interacting with GSH as a reducing reagent (Figure 10B).

In Figure 10A the protein serves as a scaffold for the disulfide substrate, allowing optimal glutathione geometry. Accordingly, the oxidative half-reaction is optimized (steps 1−4) whereas the reductive half-reaction (steps 5−8) is far less clearly defined. Please note that the second cysteine residue is not required for catalysis. The scaffold model explains why all Grxs, including enzymatically inactive monothiol Grxs, can be easily glutathionylated. It is furthermore in agreement with the observations that the reducing substrate does not have to be glutathione (RS^- can replace GS^- in steps 5−8) and that deprotonation of the weak nucleophile GSH can become rate-limiting (*27*, *31*, *33*, *37*). The solved structures of several glutathionylated Grxs could therefore reflect species V. The model also applies when the reductive half-reaction is undesired *in vivo*, for example, when Grxs sense the degree of glutathionylation of certain proteins (*5*) or serve as scaffolds for glutathione-dependent syntheses (such as iron−sulfur clusters (*57*)). In the latter case species I could interact with GSH instead of RSSG.

Nevertheless, the scaffold model does not explain why most monothiol Grxs are inactive in enzymatic assays and why reduction of *Sc*Grx7-SSG by GSH is much slower than catalytic turnover. It also does not explain why mutation of a second cysteine residue abolishes or significantly reduces activity of several Grxs *in vitro* (*10*, *30*, *35*, and this study). These phenomena are in agreement with the activator model in combination with the cysteine resolving model (Figure 10B): The cysteine thiolate residue of most if not all Grxs is probably very reactive. Thus, the oxidative half-reaction

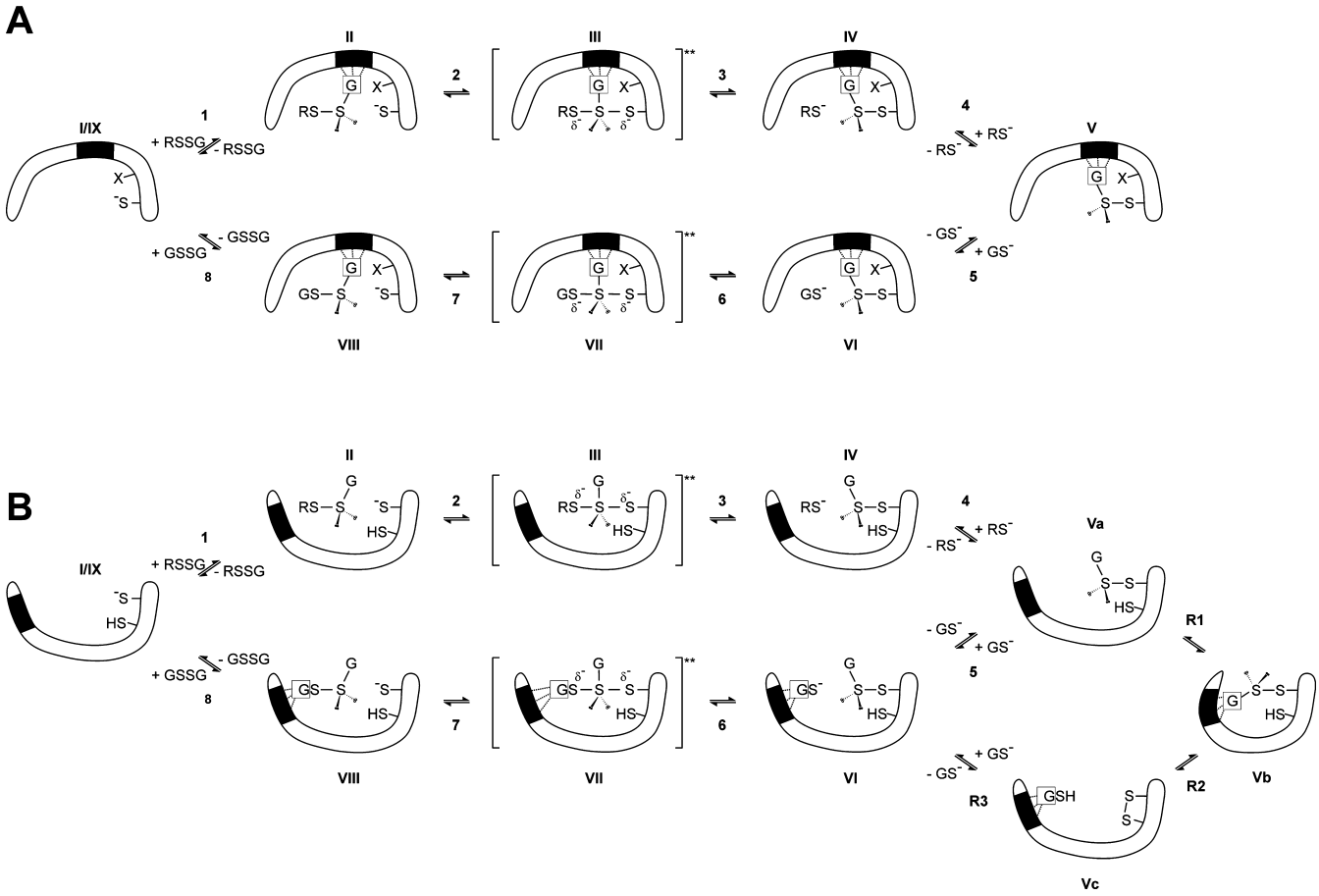

FIGURE 10: Refined models describing the catalytic mechanism of Grxs. A 180° angle between the substrate disulfide bond and the attacking protein thiolate sulfur atom is optimal to achieve the trigonal bipyramidal transition state of a S_N2 reaction (*57*). Therefore, enzyme substrate complexes are probably quite restricted in their geometry, and the glutathionyl moieties of the disulfide substrate and GSH adopt alternative positions during catalysis unless conformational changes occur. (A) For the glutathione scaffold model the glutathionyl moiety of the disulfide substrate occupies the glutathione binding site during the entire catalytic cycle. The second cysteine residue in the CxxC motif can be replaced with another amino acid. (B) For the glutathione activator model interaction of Grx with GSH during the reductive half-reaction is most important for catalysis (steps 6 and 7). The cysteine resolving model comprises reactions R1−R3 and explains the loss of activity for monothiol Grxs and some mutant dithiol Grxs. For *Sc*Grx8 step 5 does not seem to occur to a significant extent. Both models are not exclusive. See Discussion for further details.

does not necessarily require strong interactions but a correct orientation of the disulfide substrate (steps 1−3). Binding and activation of the weak nucleophile GSH (steps 6 and 7) can be critical for catalysis as shown for human Grx (*37*), and therefore, alternative GSH activator sites can result in significantly different enzymatic activities. For example, Figures 7E and 8G suggest that oxidized *Sc*Grx8 is half-saturated by GSH as a reducing agent in the lower millimolar concentration range, whereas the K_m of *Sc*Grx7 for GSH is in the middle micromolar concentration range (*12*) and might reflect an adaptation to its localization in the secretory pathway.

Stability of intermediate Va in Figure 10B is a critical point in the resolving model (steps R1−R3). Apart from the utilization of nonglutathione substrates (step 5 in Figure 1), this model provides an alternative explanation as to why some Grxs retained a second cysteine residue: After release of the first product (step 4 in Figure 10B) either the reaction can continue without any difficulties via step 5 or the covalently bound glutathione moiety can occupy the GSH activator site due to the structural identity (species Vb). If reaction R1 occurs to a significant extent (e.g., for *Sc*Grx8), the overall reaction could be slowed down because of conformational changes. In the case of many monothiol Grxs and *Sc*Grx8^{C28S}, reaction R1 could even lead to a dead-end complex if equilibrium is on the side of species Vb. This species might be a good redox sensor *in vivo*. For dithiol Grxs such as *Sc*Grx8 or special monothiol Grxs such as *Sc*Grx5 (*10*) a second cysteine residue can resolve the intermolecular disulfide bond (species Vc), and the enzyme could be reintroduced in the catalytic cycle *in vitro* and *in vivo*. In contrast to most monothiol Grxs, reaction R1 does not seem to occur in the HEDS assay with *Sc*Grx7. However, complete removal of noncovalently bound glutathione during purification of *Sc*Grx7-SSG could favor formation of species Vb. Accordingly, back-reaction R1, which does not depend on GSH, becomes rate-limiting for the reductive half-reaction of purified *Sc*Grx7-SSG (Figure 8H,J,L).

Please note that the models are not necessarily exclusive: One possibility is that there are two different glutathione interacting sites in each Grx, one scaffold site *and* one activator site. For example, one or two amino acids acting as acid−base catalysts might be sufficient for the activator site and might be replaced in several monothiol Grxs. Alternatively, if protein species V in Figure 10A (steps 1−4) undergoes a conformational change that is coupled to unbinding of the glutathione moiety, it could be converted to species V in Figure 10B (steps 5−8). In such a scenario

the scaffold and the activator site could be identical, catalyzing both half-reactions. In summary, the refined model could be useful to discriminate between the different classes of Grxs and could serve as a starting point to precisely define the catalytic mechanism(s) of Grxs.

CONCLUSION

We showed that the novel glutaredoxin *Sc*Grx8 does not contribute to general resistance against oxidative stress, has several unusual structural features, is monomeric, undergoes very slow autoxidation, accepts electrons from GSH but not TrxR, and reduces glutathionylated substrates via a dithiol mechanism. A comparison of the reductive half-reactions of *Sc*Grx8 and *Sc*Grx7 revealed great differences between both proteins. Several of our data support the theory of a conformational change during catalysis. In addition, we presented a detailed unifying model that is suited to explain most of the observed phenomena for mono- and dithiol Grxs to date.

ACKNOWLEDGMENT

The authors thank Helmut Hartl for atomic emission spectroscopy, Jan Riemer for reading the manuscript, and Prof. Walter Neupert for support. We are grateful to Chris Grant, University of Manchester, for antisera against yeast Trx1 and Trx2.

SUPPORTING INFORMATION AVAILABLE

Mass spectrometric data on *Sc*Grx7, *Sc*Grx8, and mutants (Figures S1 and S2). This material is available free of charge via the Internet at http://pubs.acs.org.

REFERENCES

1. Martin, J. L. (1995) Thioredoxin—a fold for all reasons. *Structure 15*, 245–250.
2. Herrero, E., and de la Torre-Ruiz, M. A. (2007) Monothiol glutaredoxins: a common domain for multiple functions. *Cell. Mol. Life Sci. 64*, 1518–1530.
3. Rouhier, N., Lemaire, S. D., and Jacquot, J. P. (2008) The role of glutathione in photosynthetic organisms: emerging functions for glutaredoxins and glutathionylation. *Annu. Rev. Plant Biol. 59*, 143–166.
4. Lillig, C. H., Berndt, C., and Holmgren, A. (2008) Glutaredoxin systems. *Biochim. Biophys. Acta 1780*, 1304–1317.
5. Mieyal, J. J., Gallogly, M. M., Qanungo, S., Sabens, E. A., and Shelton, M. D. (2008) Molecular mechanisms and clinical implications of reversible protein *S*-glutathionylation. *Antioxid. Redox Signaling 10*, 1941–1988.
6. Luikenhuis, S., Perrone, G., Dawes, I. W., and Grant, C. M. (1998) The yeast *Saccharomyces cerevisiae* contains two glutaredoxin genes that are required for protection against reactive oxygen species. *Mol. Biol. Cell 9*, 1081–1091.
7. Rodriguez-Manzaneque, M. T., Ros, J., Cabiscol, E., Sorribas, A., and Herrero, E. (1999) Grx5 glutaredoxin plays a central role in protection against protein oxidative damage in *Saccharomyces cerevisiae*. *Mol. Cell. Biol. 19*, 8180–8190.
8. Rodriguez-Manzaneque, M. T., Tamarit, J., Belli, G., Ros, J., and Herrero, E. (2002) Grx5 is a mitochondrial glutaredoxin required for the activity of iron/sulfur enzymes. *Mol. Biol. Cell 13*, 1109–1121.
9. Belli, G., Polaina, J., Tamarit, J., De La Torre, M. A., Rodriguez-Manzaneque, M. T., Ros, J., and Herrero, E. (2002) Structure-function analysis of yeast Grx5 monothiol glutaredoxin defines essential amino acids for the function of the protein. *J. Biol. Chem. 277*, 37590–37596.
10. Tamarit, J., Belli, G., Cabiscol, E., Herrero, E., and Ros, J. (2003) Biochemical characterization of yeast mitochondrial Grx5 monothiol glutaredoxin. *J. Biol. Chem. 278*, 25745–25751.
11. Lopreiato, R., Facchin, S., Sartori, G., Arrigoni, G., Casonato, S., Ruzzene, M., Pinna, L. A., and Carignani, G. (2004) Analysis of the interaction between piD261/Bud32, an evolutionarily conserved protein kinase of *Saccharomyces cerevisiae*, and the Grx4 glutaredoxin. *Biochem. J. 377*, 395–405.
12. Mesecke, N., Mittler, S., Eckers, E., Herrmann, J. M., and Deponte, M. (2008) Two novel monothiol glutaredoxins from *Saccharomyces cerevisiae* provide further insight into iron-sulfur cluster binding, oligomerization, and enzymatic activity of glutaredoxins. *Biochemistry 47*, 1452–1463.
13. Mesecke, N., Spang, A., Deponte, M., and Herrmann, J. M. (2008) A novel group of glutaredoxins in the cis-Golgi critical for oxidative stress resistance. *Mol. Biol. Cell 19*, 2673–2680.
14. Izquierdo, A., Casas, C., Mühlenhoff, U., Lillig, C. H., and Herrero, E. (2008) Yeast Grx6 and Grx7 are monothiol glutaredoxins associated with the early secretory pathway. *Eukaryot. Cell 7*, 1415–1426.
15. Fetrow, J. S., Siew, N., Di Gennaro, J. A., Martinez-Yamout, M., Dyson, H. J., and Skolnick, J. (2001) Genomic-scale comparison of sequence- and structure-based methods of function prediction: does structure provide additional insight? *Protein Sci. 10*, 1005–1014.
16. Ghaemmaghami, S., Huh, W. K., Bower, K., Howson, R. W., Belle, A., Dephoure, N., O'Shea, E. K., and Weissman, J. S. (2003) Global analysis of protein expression in yeast. *Nature 425*, 737–741.
17. Huh, W. K., Falvo, J. V., Gerke, L. C., Carroll, A. S., Howson, R. W., Weissman, J. S., and O'Shea, E. K. (2003) Global analysis of protein localization in budding yeast. *Nature 425*, 686–691.
18. Holmgren, A. (1979) Glutathione-dependent synthesis of deoxyribonucleotides. Purification and characterization of glutaredoxin from *Escherichia coli*. *J. Biol. Chem. 254*, 3664–3671.
19. Luthman, M., and Holmgren, A. (1982) Glutaredoxin from calf thymus. Purification to homogeneity. *J. Biol. Chem. 257*, 6686–6690.
20. Aslund, F., Ehn, B., Miranda-Vizuete, A., Pueyo, C., and Holmgren, A. (1994) Two additional glutaredoxins exist in *Escherichia coli*: glutaredoxin 3 is a hydrogen donor for ribonucleotide reductase in a thioredoxin/glutaredoxin 1 double mutant. *Proc. Natl. Acad. Sci. U.S.A. 91*, 9813–9817.
21. Vlamis-Gardikas, A., Aslund, F., Spyrou, G., Bergman, T., and Holmgren, A. (1997) Cloning, overexpression, and characterization of glutaredoxin 2, an atypical glutaredoxin from *Escherichia coli*. *J. Biol. Chem. 272*, 11236–11243.
22. Hopper, S., Johnson, R. S., Vath, J. E., and Biemann, K. (1989) Glutaredoxin from rabbit bone marrow. Purification, characterization, and amino acid sequence determined by tandem mass spectrometry. *J. Biol. Chem. 264*, 20438–20447.
23. Mieyal, J. J., Starke, D. W., Gravina, S. A., and Hocevar, B. A. (1991) Thioltransferase in human red blood cells: kinetics and equilibrium. *Biochemistry 30*, 8883–8891.
24. Lundberg, M., Johansson, C., Chandra, J., Enoksson, M., Jacobsson, G., Ljung, J., Johansson, M., and Holmgren, A. (2001) Cloning and expression of a novel human glutaredoxin (Grx2) with mitochondrial and nuclear isoforms. *J. Biol. Chem. 276*, 26269–26275.
25. Johansson, C., Lillig, C. H., and Holmgren, A. (2004) Human mitochondrial glutaredoxin reduces S-glutathionylated proteins with high affinity accepting electrons from either glutathione or thioredoxin reductase. *J. Biol. Chem. 279*, 7537–7543.
26. Berndt, C., Hudemann, C., Hanschmann, E. M., Axelsson, R., Holmgren, A., and Lillig, C. H. (2007) How does iron-sulfur cluster coordination regulate the activity of human glutaredoxin 2? *Antioxid. Redox Signaling 9*, 151–157.
27. Gallogly, M. M., Starke, D. W., Leonberg, A. K., Ospina, S. M., and Mieyal, J. J. (2008) Kinetic and mechanistic characterization and versatile catalytic properties of mammalian glutaredoxin2: Implications for intracellular roles. *Biochemistry 47*, 11144–11157.
28. Sha, S., Minakuchi, K., Higaki, N., Sato, K., Ohtsuki, K., Kurata, A., Yoshikawa, H., Kotaru, M., Masumura, T., Ichihara, K., and Tanaka, K. (1997) Purification and characterization of glutaredoxin (thioltransferase) from rice (*Oryza sativa* L.). *J. Biochem. 121*, 842–848.
29. Rahlfs, S., Fischer, M., and Becker, K. (2001) *Plasmodium falciparum* possesses a classical glutaredoxin and a second, glutaredoxin-like protein with a PICOT homology domain. *J. Biol. Chem. 276*, 37133–37140.

30. Rouhier, N., Gelhaye, E., and Jacquot, J. P. (2002) Exploring the active site of plant glutaredoxin by site-directed mutagenesis. *FEBS Lett. 511*, 145–149.
31. Zaffagnini, M., Michelet, L., Massot, V., Trost, P., and Lemaire, S. D. (2008) Biochemical characterization of glutaredoxins from *Chlamydomonas reinhardtii* reveals the unique properties of a chloroplastic CGFS-type glutaredoxin. *J. Biol. Chem. 283*, 8868–8876.
32. Deponte, M., Becker, K., and Rahlfs, S. (2005) *Plasmodium falciparum* glutaredoxin-like proteins. *Biol. Chem. 386*, 33–40.
33. Fernandes, A. P., Fladvad, M., Berndt, C., Andresen, C., Lillig, C. H., Neubauer, P., Sunnerhagen, M., Holmgren, A., and Vlamis-Gardikas, A. (2005) A novel monothiol glutaredoxin (Grx4) from *Escherichia coli* can serve as a substrate for thioredoxin reductase. *J. Biol. Chem. 280*, 24544–24552.
34. Filser, M., Comini, M. A., Molina-Navarro, M. M., Dirdjaja, N., Herrero, E., and Krauth-Siegel, R. L. (2008) Cloning, functional analysis, and mitochondrial localization of *Trypanosoma brucei* monothiol glutaredoxin-1. *Biol. Chem. 389*, 21–32.
35. Bushweller, J. H., Aslund, F., Wuthrich, K., and Holmgren, A. (1992) Structural and functional characterization of the mutant *Escherichia coli* glutaredoxin (C14→S) and its mixed disulfide with glutathione. *Biochemistry 31*, 9288–9293.
36. Gravina, S. A., and Mieyal, J. J. (1993) Thioltransferase is a specific glutathionyl mixed disulfide oxidoreductase. *Biochemistry 32*, 3368–3376.
37. Srinivasan, U., Mieyal, P. A., and Mieyal, J. J. (1997) pH profiles indicative of rate-limiting nucleophilic displacement in thioltransferase catalysis. *Biochemistry 36*, 3199–3206.
38. Yang, Y., Jao, S., Nanduri, S., Starke, D. W., Mieyal, J. J., and Qin, J. (1998) Reactivity of the human thioltransferase (glutaredoxin) C7S, C25S, C78S, C82S mutant and NMR solution structure of its glutathionyl mixed disulfide intermediate reflect catalytic specificity. *Biochemistry 37*, 17145–17156.
39. Sikorski, R. S., and Hieter, P. (1989) A system of shuttle vectors and yeast host strains designed for efficient manipulation of DNA in *Saccharomyces cerevisiae*. *Genetics 122*, 19–27.
40. Sherman, F., Fink, G. R., and Hicks, J. (1986) *Methods in yeast genetics: A laboratory course*, Cold Spring Harbor Laboratory Press, New York.
41. Bradford, M. M. (1976) A rapid and sensitive method for the quantitation of microgram quantities of protein utilizing the principle of protein-dye binding. *Anal. Biochem. 72*, 248–254.
42. Laemmli, U. K. (1970) Cleavage of structural proteins during the assembly of the head of bacteriophage T4. *Nature 227*, 680–685.
43. Davis, R. E., and Swain, C. G. (1960) General acid catalysis of the hydrolysis of sodium borohydride. *J. Am. Chem. Soc. 82*, 5949–5950.
44. Kosower, N. S., and Kosower, E. M. (1995) Diamide: an oxidant probe for thiols. *Methods Enzymol. 251*, 123–133.
45. Ellman, G. L. (1959) Tissue sulfhydryl groups. *Arch. Biochem. Biophys. 82*, 70–77.
46. Thompson, J. D., Higgins, D. G., and Gibson, T. J. (1994) CLUSTAL W: improving the sensitivity of progressive multiple sequence alignment through sequence weighting, position-specific gap penalties and weight matrix choice. *Nucleic Acids Res. 22*, 4673–4680.
47. Johansson, C., Kavanagh, K. L., Gileadi, O., and Oppermann, U. (2007) Reversible sequestration of active site cysteines in a 2Fe-2S-bridged dimer provides a mechanism for glutaredoxin 2 regulation in human mitochondria. *J. Biol. Chem. 282*, 3077–3082.
48. Guex, N., and Peitsch, M. C. (1997) SWISS-MODEL and the Swiss-PdbViewer: an environment for comparative protein modeling. *Electrophoresis 18*, 2714–2723.
49. Schwede, T., Kopp, J., Guex, N., and Peitsch, M. C. (2003) SWISS-MODEL: an automated protein homology-modeling server. *Nucleic Acids Res. 31*, 3381–3385.
50. Fladvad, M., Bellanda, M., Fernandes, A. P., Mammi, S., Vlamis-Gardikas, A., Holmgren, A., and Sunnerhagen, M. (2005) Molecular mapping of functionalities in the solution structure of reduced Grx4, a monothiol glutaredoxin from *Escherichia coli*. *J. Biol. Chem. 280*, 24553–24561.
51. Woo, J. R., Kim, S. J., Jeong, W., Cho, Y. H., Lee, S. C., Chung, Y. J., Rhee, S. G., and Ryu, S. E. (2004) Structural basis of cellular redox regulation by human TRP14. *J. Biol. Chem. 279*, 48120–48125.
52. Jeong, W., Yoon, H. W., Lee, S. R., and Rhee, S. G. (2004) Identification and characterization of TRP14, a thioredoxin-related protein of 14 kDa. New insights into the specificity of thioredoxin function. *J. Biol. Chem. 279*, 3142–3150.
53. Yang, Y. F., and Wells, W. W. (1991) Identification and characterization of the functional amino acids at the active center of pig liver thioltransferase by site-directed mutagenesis. *J. Biol. Chem. 266*, 12759–12765.
54. Nordstrand, K., Sandström, A., Aslund, F., Holmgren, A., Otting, G., and Berndt, K. D. (2000) NMR structure of oxidized glutaredoxin 3 from *Escherichia coli*. *J. Mol. Biol. 303*, 423–432.
55. Wiita, A. P., Perez-Jimenez, R., Walther, K. A., Gräter, F., Berne, B. J., Holmgren, A., Sanchez-Ruiz, J. M., and Fernandez, J. M. (2007) Probing the chemistry of thioredoxin catalysis with force. *Nature 450*, 124–127.
56. Bandyopadhyay, S., Gama, F., Molina-Navarro, M. M., Gualberto, J. M., Claxton, R., Naik, S. G., Huynh, B. H., Herrero, E., Jacquot, J. P., Johnson, M. K., and Rouhier, N. (2008) Chloroplast monothiol glutaredoxins as scaffold proteins for the assembly and delivery of [2Fe-2S] clusters. *EMBO J. 27*, 1122–1133.
57. Pappas, J. A. (1976) Theoretical studies of the reactions of the sulfur-sulfur bond. 1. General heterolytic mechanisms. *J. Am. Chem. Soc. 99*, 2926–2930.

BI801859B